

# 1 The role of föhn winds in eastern Antarctic Peninsula rapid ice shelf 2 collapse

3 Matthew K. Laffin<sup>1</sup>, Charles S. Zender<sup>1,2</sup>, Melchior van Wessem<sup>3</sup>, Sebastián Marinsek<sup>4</sup>

4 <sup>1</sup>Department of Earth System Science, University of California, Irvine, USA

5 <sup>2</sup>Department of Computer Science, University of California, Irvine, USA

6 <sup>3</sup>Institute for Marine and Atmospheric Research Utrecht (IMAU), Utrecht University, Utrecht, Netherlands

7 <sup>4</sup>Instituto Antártico Argentino, Buenos Aires, Argentina

8 *Correspondence to:* Matthew K. Laffin (mlaffin@uci.edu)

9 **Abstract.** Ice shelf collapse reduces buttressing and enables grounded glaciers to contribute more rapidly to sea-level rise in  
10 a warming climate. The abrupt collapses of the Larsen A (1995) and B (2002) ice shelves on the Antarctic Peninsula (AP)  
11 occurred, at least for Larsen B, ~~when a large~~ long period ocean swells damaged the calving fronts and the ice shelves shelf  
12 ~~was~~ inundated with melt lakes that led to ~~large~~ large-scale hydrofracture cascades. During collapse, ~~field surface~~  
13 ~~observations and satellite observations~~ indicate föhn winds were present on both ice shelves. Here we use a regional climate  
14 model and Machine Learning analyses to evaluate the contributory roles of föhn winds and associated melt events prior to  
15 and during the collapses for ice shelves on the AP. Föhn winds caused about  $25\% \pm 3\%$  of the total annual melt in just 9 days  
16 on Larsen A prior to and during collapse and were present during the Larsen B collapse which helped form extensive melt  
17 lakes ~~that surpassed a critical stability depth.~~ At the same time, the off-coast wind direction created by föhn winds helped  
18 melt and physically push sea ice away from the ice shelf calving fronts that allowed ~~large~~ long period ocean swells to reach  
19 and damage the front, which ~~has been theorised to have~~ ultimately triggered ~~the~~ collapse. Collapsed ice shelves experienced  
20 enhanced surface melt driven by föhn winds over a large spatial extent and near the calving front, whereas ~~extant~~ SCAR inlet  
21 ~~and the Larsen C~~ ice shelves are affected less by föhn wind-induced melt and do not experience ~~regular~~ large-scale melt  
22 ponds. These results suggest ~~extant SCAR inlet and the Larsen C~~ ice shelves ~~are~~ may be less likely to experience rapid  
23 collapse due to föhn-driven melt so long as surface temperatures and föhn occurrence remain within historical bounds.

## 24 1 Introduction

25 ~~The sudden disintegration of ice shelves on the eastern periphery of the Antarctic Peninsula (AP) represents the culmination~~  
26 ~~of a critical regional warming trend and anomalous surface melt in the region (Vaughan et al., 2003).~~ Ice shelves, the floating  
27 extensions of grounded glaciers, subdue the discharge of grounded ice into the global ocean (Rignot et al., 2004; Scambos et  
28 al., 2004; Gudmundsson et al., 2013; Borstad et al., 2016). Re-examination of past ice shelf collapse events can help to shed  
29 light on the mechanisms of collapse and improve the understanding of ice shelf dynamics for future projections of sea-level

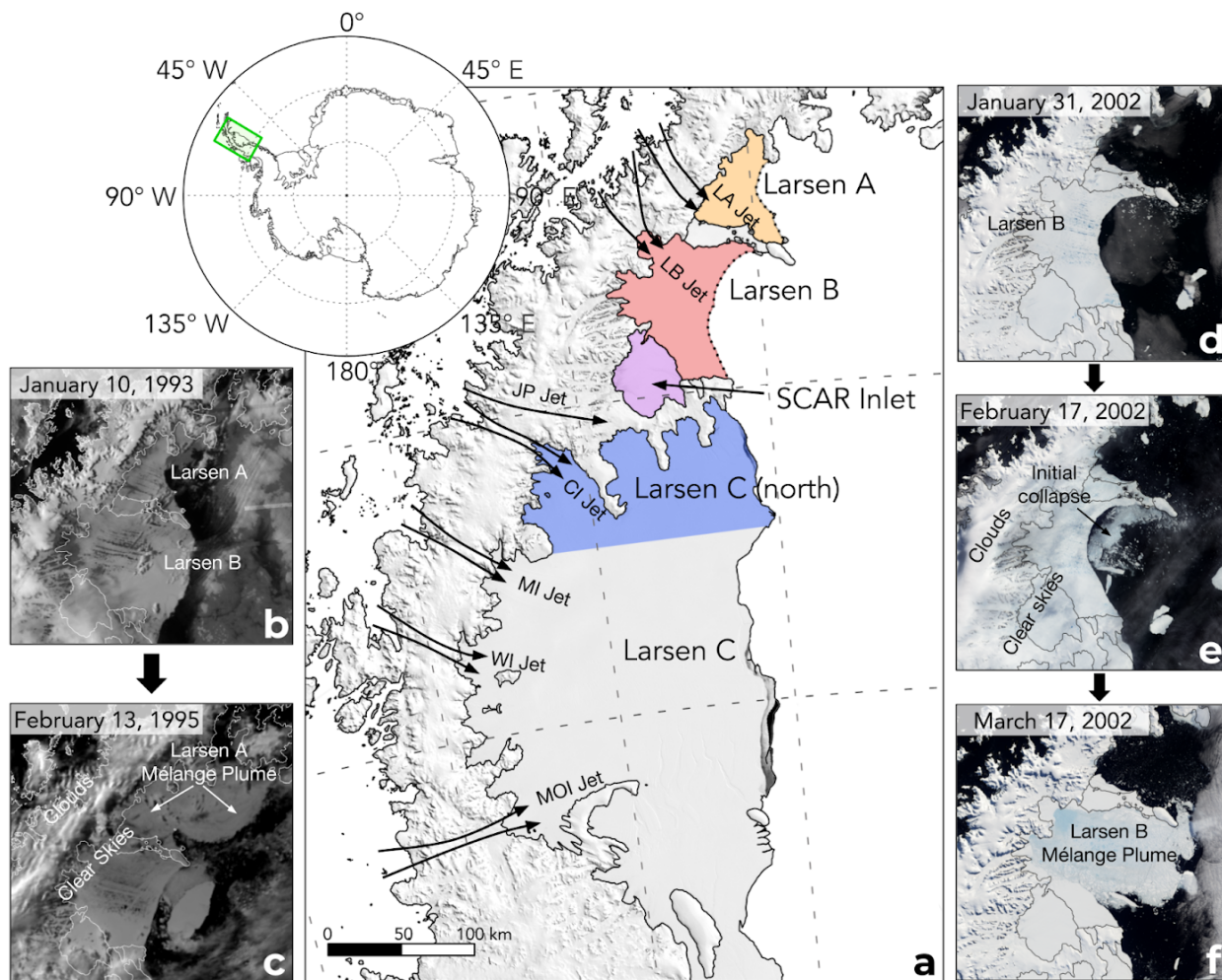
30 rise (Rignot et al., 2004; Gudmundsson et al., 2013; Borstad et al., 2016). The final collapses of the Larsen A (LAIS) in 1995  
31 and the Larsen B (LBIS) ice shelves in 2002 have been attributed to decreased structural integrity brought on by a  
32 combination of factors. Most notably, regional atmospheric warming (Scambos et al., 2000; Mulvaney et al., 2012), extended  
33 melt seasons (Scambos et al., 2003), multi-year firn pore space depletion (Kuipers Munneke et al., 2014; Trusel et al., 2015),  
34 melt pond flooding ~~and~~ (Glasser and Scambos (2008); Trusel et al., 2013; Leeson et al., 2020), crevasse expansion through  
35 hydrofracture (Scambos et al., 2003; Banwell et al., 2013; ~~Trusel et al., 2013~~; Pollard et al., 2015; Alley et al., 2018;  
36 Banwell et al., 2019; Robel and Banwell, 2019; ~~Leeson et al., 2020~~), glacier structural discontinuities (Glasser et al., 2008),  
37 basal melt (Pritchard et al., 2012; Rignot et al., 2013; Depoorter et al., 2013; Schodlok et al., 2016; Adusumilli et al., 2018),  
38 warm melt-water intrusion (Braun et al., 2009), melting of the ice melange within rifts conducive to rift propagation (Larour  
39 et al., 2021), and regional sea ice loss allowing ocean swell flexure stress on the calving front (Banwell et al., 2017; Massom  
40 et al., 2018).

41 While the list of mechanisms that can destabilise ice shelves is extensive, a conceptual model for rapid ice shelf  
42 collapse proposed by Massom et al., (2018) identifies 4 essential prerequisites for sudden collapse: (1) extensive surface  
43 flooding and hydrofracture; (2) reduced sea ice or fast ice at the ice shelf front; (3) outer margin or terminus fracturing and  
44 rifting; and (4) initial calving trigger at the ice shelf margin. ~~In addition Massom et al., (2018) concluded that a lack of~~  
45 ~~summer sea ice allowed large period ocean swells to reach the ice shelf calving front.~~ They theorise waves led to calving  
46 front damage and small calving events that breached the “compressive arch” of stability of both ice shelves proposed by  
47 Doake et al., (1998). At the same time the ice shelves were covered in extensive surface melt lakes that were unlikely to  
48 drain horizontally because of the relatively flat surface (Banwell et al., 2014). Satellite observations and ice shelf stability  
49 model studies determined the LBIS was covered with >2750 melt lakes that were on average 1 meter deep before collapse  
50 ~~which corresponds to a possible melt lake depth stability threshold for ice shelves in the region~~ (Glasser and Scambos  
51 (2008); Banwell et al., 2013). Ice shelves inundated with surface melt lakes are susceptible to disintegration through a  
52 process known as hydrofracture, where meltwater applies outward and downward pressure to the walls and tip of crevasses  
53 that can propagate through the ice shelf (Scambos et al., 2003; Banwell et al., 2013; Bell et al., 2018; Lhermitte et al., 2020).  
54 Furthermore, melt lakes ~~at critical water depths that rapidly drain by hydrofracture~~ can create fracture patterns that split ice  
55 shelves into sections with aspect ratios that support unstable rollover, and hydrofracture cascades that begin when melt lakes  
56 drain and/or calving occurs at the ice shelf terminus (Scambos et al., 2003; Banwell et al., 2013; Burton et al., 2013; Robel  
57 and Banwell ~~(, 2019)~~). The combination of ocean swell stress on the calving front and extensive melt ponds led to large  
58 -scale hydrofracture cascades that proposed by Massome et al., (2018) ultimately caused the rapid collapse of ~~the LAIS~~  
59 and possibly the LBIS.

60 In addition to a lack of sea ice and extensive melt ponds, meteorological and satellite observations identify clear  
61 skies and warm west/northwest föhn wind at the time of collapse (Figure 1bc-f) (Rott et al., 1998; Rack and Rott (2004);

62 Cape et al., 2015; Massom et al., 2018). Föhn winds form when relatively cool moist air is forced over a mountain barrier,  
63 often leading to precipitation on the windward side of the barrier that dries the air mass (Grosvenor et al., 2014; Elvidge et  
64 al., 2015). As the now drier air descends the leeward slope it warms adiabatically and promotes melt directly through  
65 sensible heat exchange, and indirectly by the associated clear skies that allow additional shortwave radiation to reach the  
66 surface in non-winter months (Turton et al., 2017, 2018; Kuipers Munneke et al., 2018; Elvidge et al., 2020; Laffin et al.,  
67 2021). Föhn winds and their capacity to cause surface melt have been studied extensively on the AP. Observations and model  
68 studies on the LCIS confirm the föhn mechanism that enhances sensible heat and shortwave radiation and alters local albedo  
69 which can increase surface melt rates upwards of 50% compared to non-föhn conditions (Cape et al., 2015; Elvidge et al.,  
70 2015; King et al., 2015, 2017; Kuipers Munneke et al., 2012, 2018; Bevan et al., 2017; Lenaerts et al., 2017; Datta et al.,  
71 2019; Kirchgaessner, et al., 2021; Laffin et al., 2021, Wang et al., 2021). Late season föhn melt reduces firn pore space, and  
72 thus pre-conditions ice shelves to form melt ponds and are responsible for the increased firn density pattern east of the AP  
73 mountains on the LCIS (Holland et al., 2011; Kuipers Munneke et al., 2014; Datta et al., 2019). Föhn melt climatology  
74 studies have aimed to identify how much melt is caused by föhn and the locations most affected and found föhn winds  
75 account for up to 17 % of melt and are concentrated in the LCIS inlets (Turton et al., 2017; Datta et al., 2019; Laffin et al.,  
76 2021). Pressure gradient differences across the AP range lead to föhn winds that funnel through mountain gaps as highly  
77 concentrated föhn jets, particularly in inlets east of the AP range (Luckman et al., 2014; Elvidge et al., 2015; Kuipers  
78 Munneke et al., 2012; Grosvenor et al., 2014). In addition to enhancing surface melt rates, föhn winds exert force on sea/ice  
79 ice and drag it away from the calving front, thereby exposing the front to ocean waves (Bozkurt et al., 2018). Climatic  
80 studies of the Larsen B embayment indicate that föhn winds were coincident with collapse (Rack and Rott (2004); Leeson et  
81 al., 2017). However, it is unknown if concentrated föhn jets spilled onto the former LAIS and LBIS and, if so, whether those  
82 föhn winds contributed to their collapse. The questions, therefore, arise: 1) To what extent ~~does~~ föhn-induced melt  
83 contribute to the surface melt budget on ~~the each eastern AP ice shelf, specifically LAIS and LBIS?~~; 2) Did föhn winds and  
84 associated melt play a role in triggering the collapses of the LAIS and LBIS?; 3) What are the implications of föhn-induced  
85 melt for the remaining eastern AP ice shelves?

86 To address these questions we consider three metrics: Section 3.1 explores the total annual surface melt quantity  
87 induced by föhn winds and how melt is spatially distributed across each ice shelf; Section 3.2 identifies the coincidence of  
88 föhn-induced melt preceding and during the collapse events, and the estimated melt-lake depth in response to melt events.;  
89 Section 3.3 identifies the contribution of föhn melt to the climatological surface liquid water budget comparing collapsed and  
90 extant ice shelves ~~on the eastern AP~~. By constructing a timeline of melt and melt mechanisms and comparing melt metrics  
91 with collapsed and extant ice shelves, we can ~~identify~~ identify the contributory factors to collapse.



93 **Figure 1.** Map of the northern Antarctic Peninsula (a) showing locations of collapsed ice shelves (LAIS-January 25, 1995, LBIS-February  
 94 9, 2002), extant ice shelves (SCAR inlet and LCIS), and föhn jets (Larsen A jet (LA jet), Larsen B jet (LB jet), Jason Peninsula jet (JP jet),  
 95 Cabinet inlet jet (CI jet), Mill inlet jet (MI jet), Whirlwind inlet jet (WI jet), Mobil Oil inlet jet (MOI jet)) with a MODIS Mosaic overlay.  
 96 The colored regions indicate how this study separates ice shelves for climatic analysis. The dotted lines show the former extent of the  
 97 Larsen A and Larsen B ice shelves at the time of collapse. Panels (b)-(f) are satellite images of the collapses of the LAIS and LBIS. (b)  
 98 AVHRR (Advanced Very High-Resolution Radiometer) image of the northern AP two years before the collapse of the LAIS showing melt  
 99 lakes on the surface of both ice shelves. (c) AVHRR image after the collapse of the LAIS. (d) NASA provided MODIS (Moderate  
 100 Resolution Imaging Spectroradiometer) image showing the LBIS days before collapse began. (e) MODIS image showing a föhn wind  
 101 event (clouds over the western AP, clear skies over the ice shelves) along with the initial collapse of the LBIS. (f) MODIS image of the  
 102 complete collapse of the LBIS.

## 103 **2 Data and methods**

### 104 **2.1 Regional Climate Model 2 Simulation (RACMO2)**

105 We base our analysis on 3-hourly output from simulations by the Regional Atmospheric Climate Model 2 (RACMO2),  
106 version 2.3p2, with a horizontal resolution of 5.5km (0.05°) focused on the AP from 1979-2018. RACMO2 uses the physics  
107 package CY33r1 of the ECMWF Integrated Forecast System (IFS)  
108 (<https://www.ecmwf.int/en/elibrary/9227-part-iv-physical-processes>\textit{{ECMWF-IFS,} 2008}) in combination with  
109 atmospheric dynamics of the High-Resolution Limited Area Model (HIRLAM). When RACMO2 surface simulations are  
110 compared with AWS observations on the LCIS, surface air temperature has a slight warm bias likely because of model  
111 resolution and shortwave/longwave radiation are over/under estimated due to underestimation of clouds and moisture but  
112 overall reproduce surface observations (King et al., 2015; Leeson et al., 2017; Bozkurt et al., 2020; Laffin et al., 2021)  
113 ~~RACMO2 has been evaluated against numerous surface observations in locations all over the AP and has trouble simulating~~  
114 ~~very high and low temperature extremes in the region but is considered a good representation of surface conditions (Leeson~~  
115 ~~et al., 2017; Laffin et al., 2021).~~

### 116 **2.2 Föhn wind detection**

117 We use the Föhn Detection Algorithm (FöhnDA) that identifies föhn winds that cause melt using 12 Automatic Weather  
118 Stations (AWS) on the AP previously developed and detailed in Laffin et al., (2021). FöhnDA identifies föhn-induced melt  
119 events using binary classification Machine Learning when 10 metre air temperature (T) is greater than 0°C, which ensures it  
120 captures föhn events that cause surface melt. Thresholds for relative humidity (RH) and wind speed (WS) are more dynamic  
121 because high wind speeds and low relative humidity do not guarantee temperatures above freezing, they only aid to identify  
122 föhn. FöhnDA uses quantile regression to identify these variable thresholds that take into account the climatology and  
123 seasonality at each AWS site. FöhnDA uses two empirically determined thresholds: the 60th percentile wind speed and 30th  
124 percentile relative humidity which are 2.85 m/s and 79% averaged at all AWS locations. We co-locate AWS with the  
125 nearest model grid cell and use FöhnDA results to train a ML model that detects föhn winds in RACMO2 output. Our ML  
126 model improves the accuracy of föhn detection by over 23% when compared to the simple binary classification method  
127 applied to RACMO2 output as described above. A sensitivity study detailed in Laffin et al., (2021) compares previous föhn  
128 detection methods (Cape et al., 2015; Datta et al., 2019) and shows that FöhnDA ~~is the most accurate detection method and~~  
129 allows us to use in situ observations from AWS and expand föhn detection with RACMO2 output to regions and times when  
130 AWS observations are not available (Figure S1) (Table S1).

131 Föhn jet locations were identified using wind direction and strength during föhn events (Figure 2a) and by the  
132 surface melt pattern during föhn (Figure 3b). The RACMO2 topography pixel size is 5.5 km which is sufficient to produce  
133 the föhn jets identified on the LCIS (Elvidge et al., 2015), and allows for new föhn jet identification on the LAIS and LBIS  
134 despite lack of direct observation. However, ~~small-scale~~ föhn winds funnelled through local canyons and mountain gaps  
135 smaller than 5.5 km are not directly simulated. Therefore, we consider RACMO2 simulated estimates of surface melt caused  
136 by föhn winds to be conservative and likely ~~higher~~ **greater** in regions where föhn winds are funnelled and concentrated.

### 137 **2.3 Ice shelf intercomparison analysis**

138 We split the ice shelves into areas shown in Figure 1a (Larsen A, Larsen B, SCAR inlet, Larsen C (north), and Larsen C) and  
139 take the average of all model grid cells annually to create a climatology of surface melt, melt rate, melt hours, surface  
140 temperature. We use a two-tailed t-test statistic to identify if the mean surface temperature and mean surface melt of both ice  
141 shelves are statistically different from one another at the 95% confidence interval. We compare all ice shelves to the LBIS  
142 because it was the most recent collapse event and is adjacent to collapsed and existing ice shelves. Qualitatively similar  
143 results are obtained when comparing all ice shelves to the LAIS.

144 To compare ice shelf liquid water budgets we use a liquid-to-solid ratio (LSR) as a crude proxy for available firm air  
145 content and can be estimated as,

$$146 \quad LSR = \frac{\text{Total liquid water (snowmelt + liquid precipitation)}}{\text{Total solid precipitation (snow)}} \quad (1)$$

148  
149 where areas with  $LSR < 1$  represent an ice shelf that receives more solid precipitation than liquid water and is therefore less  
150 likely to saturate with liquid water and form melt lakes than areas with  $LSR > 1$ .

### 151 **2.4 Sea ice concentration analysis**

152 We used 3-hourly meteorological data of sea ice concentration from the European Center for Medium-Range Weather  
153 Forecasts (ECMWF) ERA5 reanalysis (Copernicus Climate Change Service, 2017). These data are available at a horizontal  
154 resolution of about 30 km or  $0.28^\circ$ . ERA5 is created by assimilated satellite and in situ observations into ECMWF's  
155 Integrated Forecast System (IFS). We compare sea ice concentration to the occurrence of föhn wind events to identify how  
156 föhn winds impact sea ice concentration. We measure the mean sea ice concentration of the ocean 90km directly east of each  
157 ice shelf (Larsen A, Larsen B, and Larsen C) in the Weddell Sea. We explore the relationship of föhn wind occurrence and  
158 sea ice concentration using a statistical pearson correlation method. When föhn winds are present we compare the mean of  
159 all sea ice concentration pixels in the designated ice shelf region for all years from 1979 to 2002. .

160

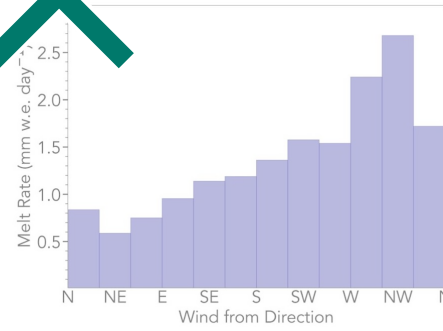
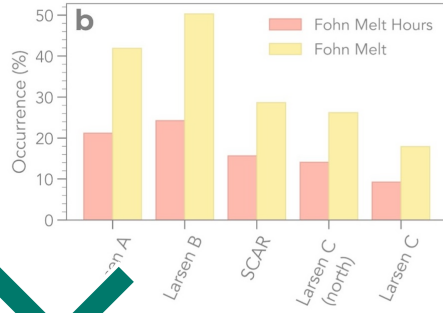
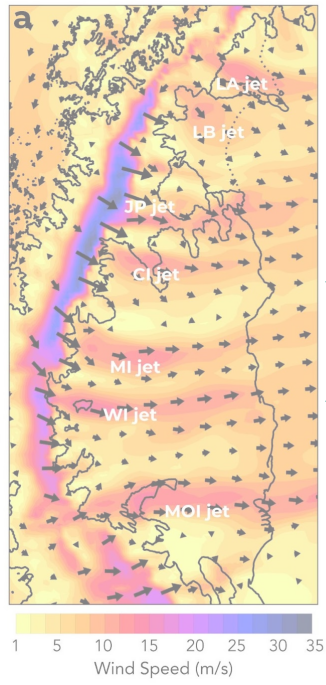
## 161 **3 Results**

### 162 **3.1 Föhn jets and melt**

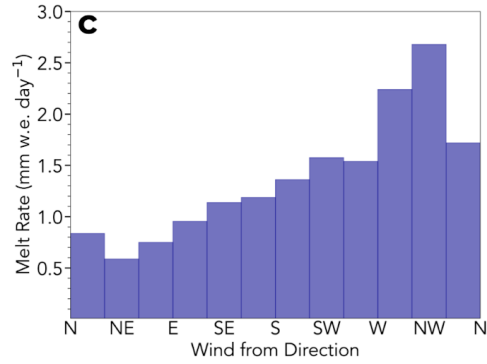
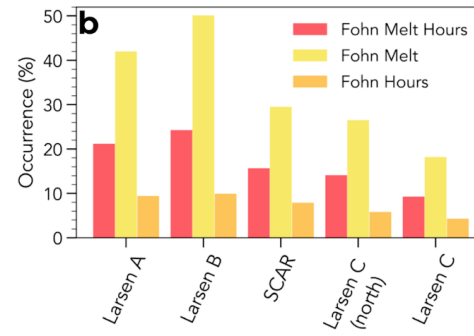
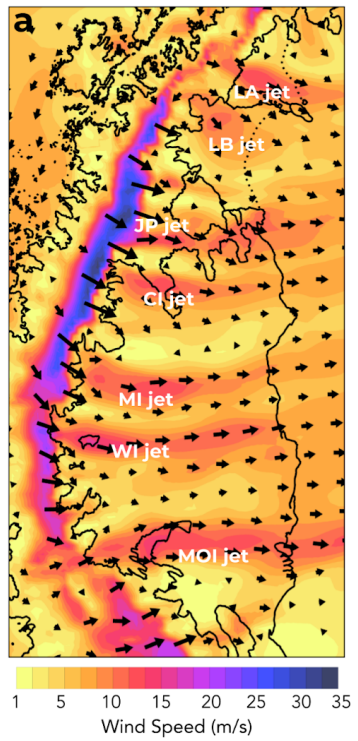
163 Using RACMO2 historical simulations, informed by a Machine Learning algorithm (**FöhnDA**) that is trained with AWS  
164 observations (Laffin et al., 2021), we identify seven recurring föhn jets or “gap winds” that lead to high surface melt rates on  
165 the eastern AP ice shelves (Figure 2a). Four of these jets (CI, MI, WI, MOI) have been studied using airborne observations  
166 and model simulations (Grosvenor et al., 2014; Elvidge et al., 2015). The remaining three jets (LA, LB, and JP) are, to our  
167 knowledge, identified here for the first time. Overall, winds from the west and northwest direction lead to increased surface  
168 melt rates that can be up to 53% higher than melt when the wind is from other directions (Figure 2c) (van den Broeke  
169 (2005)). Additionally, the degree to which föhn winds impact surface melt on each ice shelf varies depending on föhn jet  
170 **existence**, location, and wind strength (Wiesennecker et al., 2018). These variations **in föhn jet location** may provide insight  
171 into why SCAR inlet and the LCIS remain intact while the LAIS and LBIS have collapsed other than the significant  
172 difference in annual surface temperature (Cook and Vaughan (2009); Bozkurt et al., 2020; Carrasco et al., 2021).

173

174



175



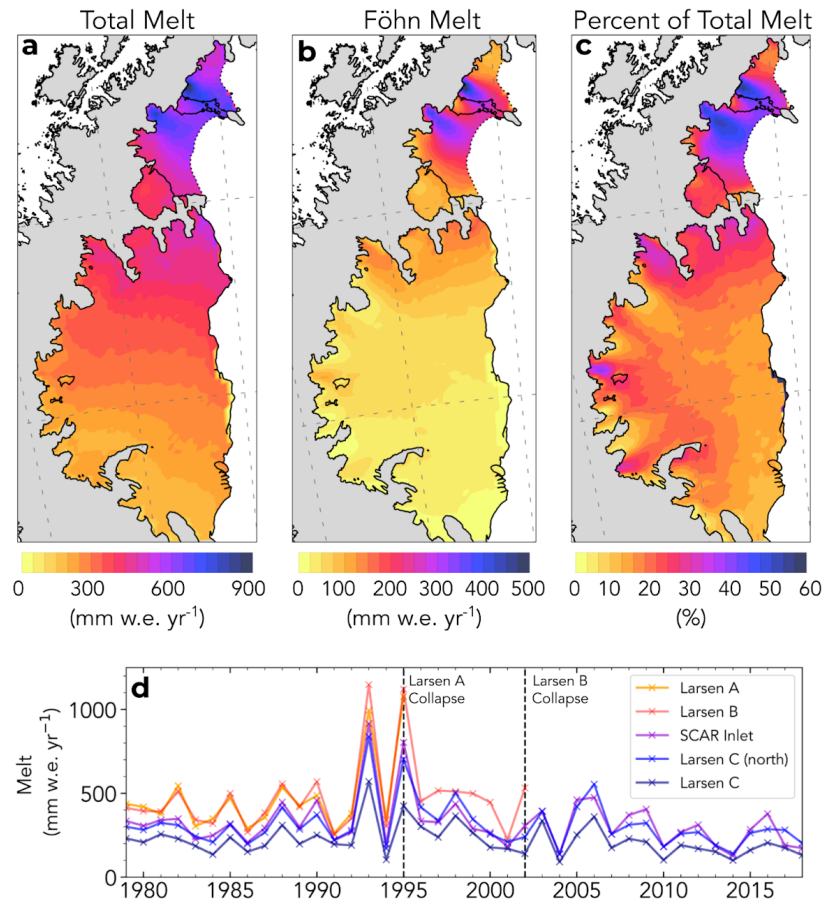


176 **Figure 2.** (a) The northern AP showing the RACMO2-simulated wind speed and direction vectors on January 24, 1995, just before the  
177 collapse of the LAIS. Föhn jet locations are indicated with names. (b)– RACMO2 annual average föhn melt hour percent of total melt  
178 hours ~~and~~, föhn melt percent of total melt for each ice shelf from, ~~and~~ percent of total hours föhn winds occur from 1980-2002. (c)  
179 RACMO2 melt rate as a function of wind direction averaged for all ice shelf regions on the AP from 1980-2002.

180

181 Surface melt production is more pronounced under the influence of föhn jets, particularly for the LA and LB jets  
182 which produce 35.7% and 31.8% more melt respectively compared to regions not in the path of a föhn jet on each ice shelf  
183 (Figure 3). Föhn-induced surface melt accounts for 42% of the total annual melt between 1979 and 2002 on the LAIS and  
184 51% of total melt on the LBIS but only represents 21% and 25% of total melt hours on the LAIS and LBIS (Figure 2b, 3c).  
185 In locations directly influenced by föhn jets, the mean annual föhn-induced melt was as high as 61% on the LAIS and 57%  
186 on the LBIS of total annual melt. By contrast, föhn-induced melt accounts for only 25% of 1979-2002 total melt on SCAR  
187 inlet and 17% on the LCIS. SCAR inlet is not directly impacted by a föhn jet, but still experiences clear skies and weak föhn  
188 influence from the overall descending air during föhn events. The LCIS is affected by numerous föhn jets (CI, MI, WI,  
189 MOI), accounting for up to 40% of the total annual melt in Cabinet and Whirlwind inlets, decreasing with distance east of  
190 the AP mountains. The stark contrast in surface melt amount and fraction caused by föhn winds on collapsed vs. intact ice  
191 shelves implicates föhn melt as a contributor to the LAIS and LBIS collapses. A clearer picture of the role of föhns emerges  
192 after we examine föhn-induced melt extent and timing.

193 The spatial distribution and extent of surface melt influence ice shelf stability. Surface melt and melt lakes near the  
194 ice shelf terminus can lead to calving front collapse and structural instability for the remaining portion of the ice shelf  
195 (Depoorter et al., 2013; Pollard et al., 2015). Consistent with this mechanism, the LA and LB föhn jets impact a large spatial  
196 area of the LAIS and LBIS, and reach the ice shelf calving fronts (Figure 3b). SCAR Inlet lacks a strong föhn jet/influence  
197 and does not regularly experience large-scale melt lakes even during high melt years (Figure 1b-f). This helps explain why  
198 SCAR Inlet is still intact, despite ~~decreased sea ice buttress force and~~ major structural changes observed after the collapse of  
199 the LBIS (Borstad et al., 2016; Qiao et al., 2020). LCIS on the other hand is impacted by four major jets and regularly  
200 experiences föhn-induced melt lakes, particularly in Cabinet inlet. ~~However, the vast size of the LCIS does not allow the~~  
201 ~~föhn-induced melt to reach the terminus.~~ However, the vast size of the LCIS limits the amount of föhn-induced melt at the  
202 terminus. The föhn melt mechanism breaks down by mixing with cold air which reduces the intensity of the föhn jets from  
203 their peak at the base of the AP mountains to the calving front (Figure 3b) (Elvidge et al., 2016; Turton et al., 2018). Having  
204 established that föhn winds significantly enhanced surface melt overall (Cape et al., 2015; Elvidge et al., 2015; Datta et al.,  
205 2019) and at the crucial calving front of LAIS and LBIS, we now examine the timing of föhn-induced melt events relative to  
206 collapse.



208 **Figure 3.** (a) RACMO2 average annual melt from 1980-2002. (b) RACMO2 average annual föhn wind-induced melt from 1980-2002. (c)  
 209 RACMO2 percent of total melt concurrent with föhn wind from 1980-2002. (d) RACMO2 time series of the mean annual surface melt on  
 210 each ice shelf from 1979-2018. Dashed vertical lines indicate the year in which each ice shelf collapsed. Note: The Larsen B [curve](#)  
 211 often overlaps the Larsen A curve.

## 212 3.2 Coincidence of föhn winds with collapse

### 213 3.2.1 LAIS

214 Three föhn wind events occurred on LAIS between January 18 and 27, 1995, overlapping with the initial phase of the LAIS  
 215 collapse that began on January 25 (Figure 4b) (Rott et al., 1998). These föhn events helped contribute to the collapse of the  
 216 ice shelf in two ways: (1) [Enhanced surface melt rates caused by the LA jet led to extensive melt lakes across the ice shelf](#)  
 217 [that possibly promoted large-scale hydrofracture cascades because of the rapid \(days to weeks\) nature of collapse \(Banwell](#)  
 218 [et al., 2013\); \(2\) The west/northwest wind direction actively pushed or melted sea ice and fast ice away from the calving](#)  
 219 [front, allowing ocean waves to reach the ice shelf terminus \(Rott et al., 1996; Massom et al., 2018\); \(2\). ~~Enhanced surface~~](#)

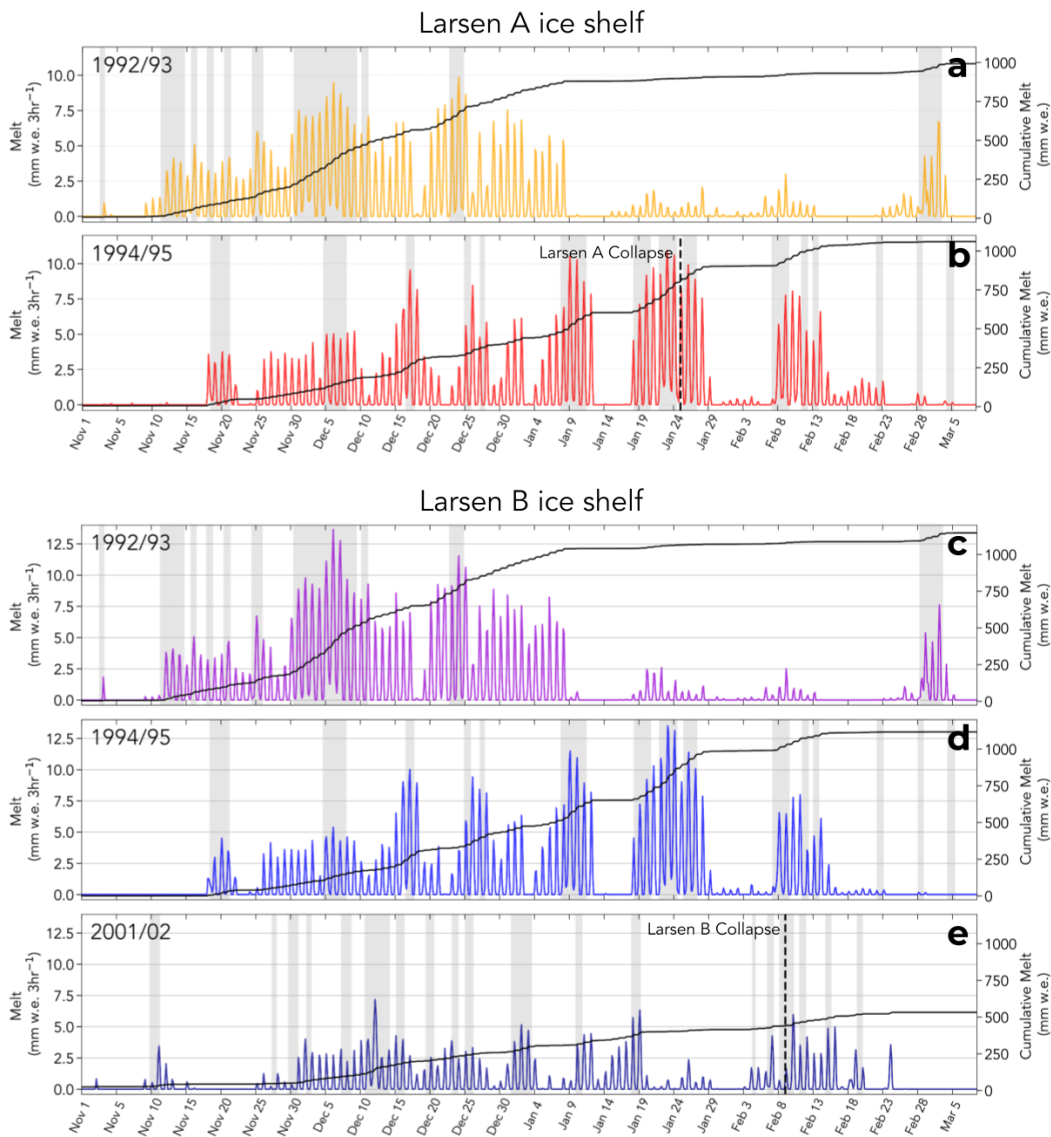
220 melt rates caused by the LA jet led to extensive melt lakes across the ice shelf that promoted large scale hydrofracture  
221 cascades when the ice shelf terminus was breached (Banwell et al., 2013). The föhn wind events prior to and during collapse  
222 lasted an average of 3 days each and produced increased surface melt greater than any other 9-day period from 1979-2018,  
223 with mean cumulative melt of 268.5 mm w.e. or 25.2% of the total annual melt in the 1994/95 melt season. Total melt during  
224 the 1994/95 melt season was 127% higher than an average year (474 mm w.e./yr) and the 9-day föhn wind event produced  
225 57% of the total melt of an average melt year. Therefore this 9-day föhn-induced melt event and melt year are clearly  
226 anomalous in the observational record. We also identify a negative correlation between the occurrence of föhn winds and sea  
227 ice concentration on all eastern AP ice shelves (Figure 5a), that is more correlated with föhn wind occurrence and air  
228 temperature (Figure 5b). When föhn winds occur on the AP, sea ice concentration decreases which is consistent with other  
229 wind types in Antarctica (katabatic winds) that form perennial wintertime polynya (Figure 5c-e)(Bromwich, 1984; Bozkurt  
230 et al., 2018; Wang et al., 2021). At the start of the 9-day föhn event, sea ice concentration east of the LAIS was at or near  
231 100% but by the time collapse began, sea ice concentration dropped significantly (Figure 5d-e).

232 We next examine the contribution of föhn-generated melt to other observables implicated in the collapse, namely  
233 surface liquid water, melt lake depth, and melt lake extent (Scambos et al., 2003). We estimate the spatial extent and depth of  
234 melt lakes prior to collapse on the LAIS using satellite images of melt lake surface area combined with model-simulated  
235 available liquid water volume. The cumulative spatial melt pattern between January 18 and 27, 1995 identifies significant  
236 melt on the LAIS ranging from 157-356 mm w.e. (Figure S2a), varying spatially with the influence of the LA jet. Satellite  
237 imagery of the LAIS during the collapse in progress show melt lakes were present (Figure S3) however because the collapse  
238 had already begun, it is likely many of the lakes had drained or had been altered so estimating melt lake extent is not  
239 possible. However, Advanced Very High-Resolution Radiometer (AVHRR) imagery on December 8, 1992, provides  
240 high-resolution cloudless images of the ice shelf taken at the end of a similar föhn-induced melt event during a year when  
241 melt was comparable to the 1994/95 melt season, therefore we consider this melt lake extent analogous to the 1994/95 melt  
242 season (Figure 4a). We find the melt lake surface area was likely between 5.1%-10.8% (103 km<sup>2</sup> - 219 km<sup>2</sup>) of the total LAIS  
243 surface area (Figure S2b). Melt lake surface area is likely underestimated because the image was taken early in the 1992/93  
244 melt season and does not easily identify small lakes or river systems. Liquid water pooling on the ice surface is modulated by  
245 the local topography. If we assume all the available surface liquid water during the 9-day melt period, minus evaporation,  
246 runoff, and refreeze, forms lakes that cover the same estimated surface area as the 1992/93 melt season, we can estimate melt  
247 lake depth during the initial collapse. We find mean melt lake depth to be between 1.38-6.86 meters depending on lake  
248 location and föhn influence, which exceeds the average lake depth of the LBIS lakes prior to collapse (1-meter) (Banwell  
249 et al., 2014) and the critical lake depth that was modelled lake depth (5m) that could lead to large-scale hydrofracture  
250 cascade identified in LBIS collapse modelling studies (3-5 m)s especially under the influence of the LA jet (Banwell et al.,  
251 2013).

252

### 253 **3.2.2 LBIS**

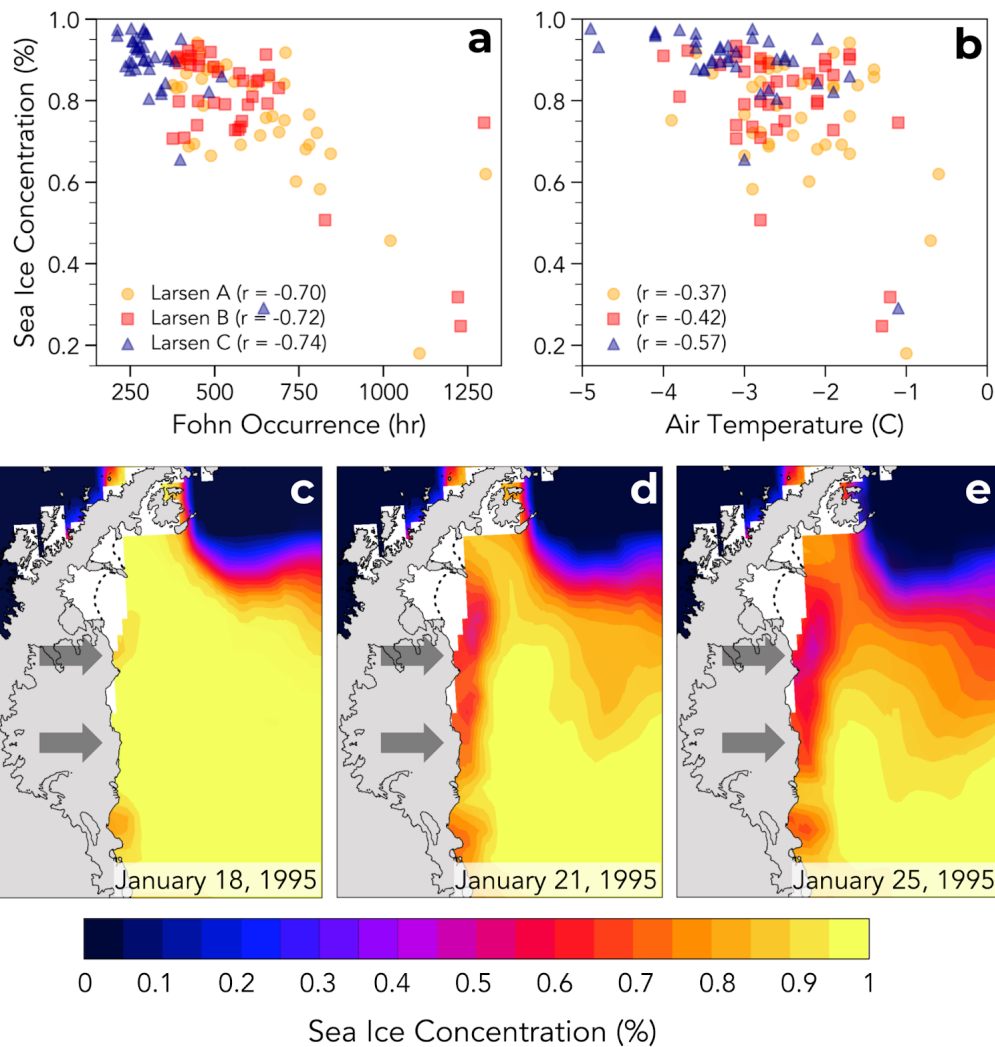
254 A föhn wind event coincided with the initial LBIS collapse on February 9, 2002, with two events just prior to collapse and  
255 three additional events before complete collapse by March 17, 2002 (Figure 4c). Föhn events in the LBIS 2001/02 melt  
256 season were relatively short, averaging less than 24 hours per event, and produced melt rates 27% higher than non-föhn melt  
257 that year and 39% of the average föhn melt rate in all other years (Figure 4e). Similar to the LAIS collapse the off-coast wind  
258 direction and enhanced surface melt rates during the föhn wind event helped push sea ice away from the calving front and  
259 contributed to surface melt lakes that led to hydrofracture and collapse (Figure 5a) (Massom et al., 2018). Additionally,  
260 previous high melt rate föhn events such as those in the 1992/93 and 1994/95 melt seasons likely preconditioned the LBIS  
261 through firn densification to support melt lake formation, discussed in section 3.3.



262

263 **Figure 4.** RACMO2 time series of surface melt production and cumulative melt during the Antarctic melt season averaged over the  
 264 indicated ice shelf. Grey shading indicates the presence of föhn winds. (a) 1992/1993 LAIS. (b) 1994/1995 LAIS. (c) 1992/1993 LBIS. (d)  
 265 1994/1995 LBIS. (e) 2001/2002 LBIS. *Note:* Surface melt that occurs after the collapse events indicated by the dashed vertical lines in (b)  
 266 and (e) are estimates of melt quantity if the ice shelves did not disintegrate.

267



268

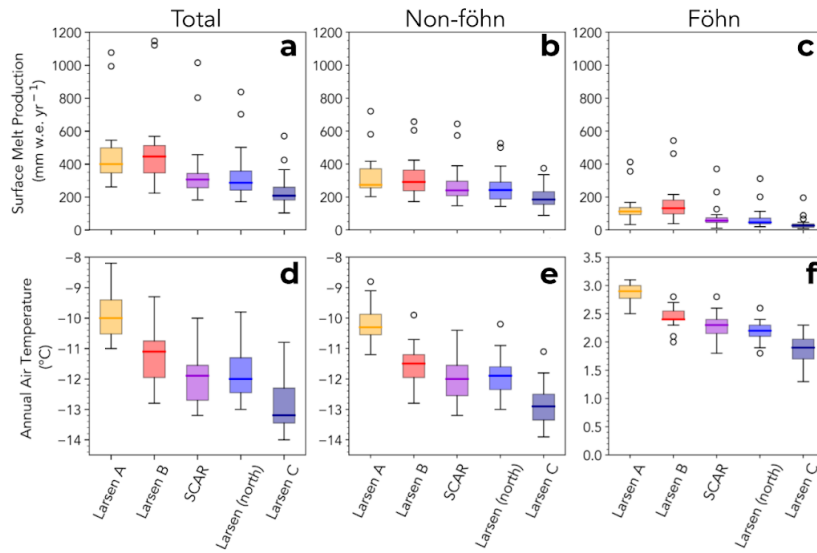
269 **Figure 5.** (a) Scatter plot of ERA5 sea ice concentration and RACMO2 identified föhn occurrence hours. (b) Scatter plot of ERA5 sea ice  
 270 concentration and RACMO2 mean summer air temperature. ERA5 sea ice concentration at the start of a 9-day föhn melt event (c), the  
 271 middle of the event (d), and on the day of initial phase of the LAIS collapse (e). Grey arrows indicate the mean föhn wind direction.

### 272 3.3 Föhn melt and the surface liquid water budget

273 To better understand the role that föhn winds play in eastern AP ice shelf surface melt and stability we intercompare melt  
 274 climatologies and the surface liquid water budget of all major eastern AP ice shelves (Larsen A, Larsen B, SCAR inlet,  
 275 Larsen C). A comparison of collapsed with intact ice shelves yields a clearer picture of the effects föhn winds have on ice  
 276 shelf stability. We identify whether annual surface melt production, melt rate, melt hours, and surface temperature variables  
 277 from 1980-2002 are significantly different from the LBIS (Figure 56 and corresponding two-tailed t-test statistics in Table

278 S2). We compare to LBIS because it was centred between other ice shelves and was the most recent to collapse. Total surface  
279 melt production on every ice shelf except LAIS differs significantly from LBIS melt (Mean annual melt over the ice shelf  
280 area; LAIS-476 mm w.e., LBIS-479 mm w.e., SCAR-353 mm w.e., Larsen(north)-336 mm w.e., LCIS-238 mm w.e.) (Figure  
281 56a), which is expected when we consider the latitudinal location and mean annual air temperature (Figure 56d) (Table S2).  
282 However, when föhn-induced melt is subtracted from total melt, the mean annual surface melt production on SCAR inlet and  
283 Larsen C (north) are not statistically different from the LBIS (LAIS-337 mm w.e., LBIS-321 mm w.e., SCAR-286 mm w.e.,  
284 Larsen(north)-278 mm w.e., LCIS-203 mm w.e.) (Figure 56b). In other words, with the exception of föhn-induced melt  
285 (Figure 56c), melt production on SCAR Inlet and LCIS are statistically indistinguishable at the 95% confidence interval from  
286 LBIS melt production. Föhn wind-induced surface melt impacted collapsed ice shelves significantly more than ~~extant ice~~  
287 ~~shelves~~ SCAR inlet and the LCIS which further defines föhn melt as an important contributor to LAIS and LBIS melt budget.

288 Our analysis of firm density or available firm pore space identifies significant differences in ice shelves that have  
289 collapsed (LAIS, LBIS) and those that remain intact (SCAR inlet, LCIS). ~~Firm densification occurs when the liquid water~~  
290 ~~fills the pore space between snow/ice crystals decreasing the air content in the firm, which forms refrozen ice layers that~~  
291 ~~promote melt lake formation (Kuipers Mummeke et al., 2012; Polashenski et al., 2017).~~ The liquid-to-solid ratio (LSR) is a  
292 crude proxy for available firm air content with extant ice shelves (SCAR inlet, LCIS) have an LSR just above 1 for the period  
293 1980-2002 if all surface melt is included (Figure 67a). The LSR for LAIS and LBIS is also just above 1 for this period,  
294 though only if föhn-induced surface melt is excluded (Figure 7b). When surface melt caused by föhn wind is included, LSR  
295 exceeds 1.5 throughout extensive regions, including the ice shelf margins, of the LAIS and LBIS. Thus the collapsed ice  
296 shelves experienced climatological LSRs significantly larger than the ~~extant ice shelves~~ SCAR inlet and the LCIS, mainly  
297 due to föhn-induced melt. ~~It is important to note that there is evidence that the LCIS experiences regions of firm densification~~  
298 ~~through melt processes, however these regions are mostly focused close to the AP mountains, likely formed from the~~  
299 ~~location of fohn jets (Hubbard et al., 2016).~~ This result suggests that föhn-induced melt helped precondition the LAIS and  
300 LBIS to produce extensive melt lakes by long-term firm densification.

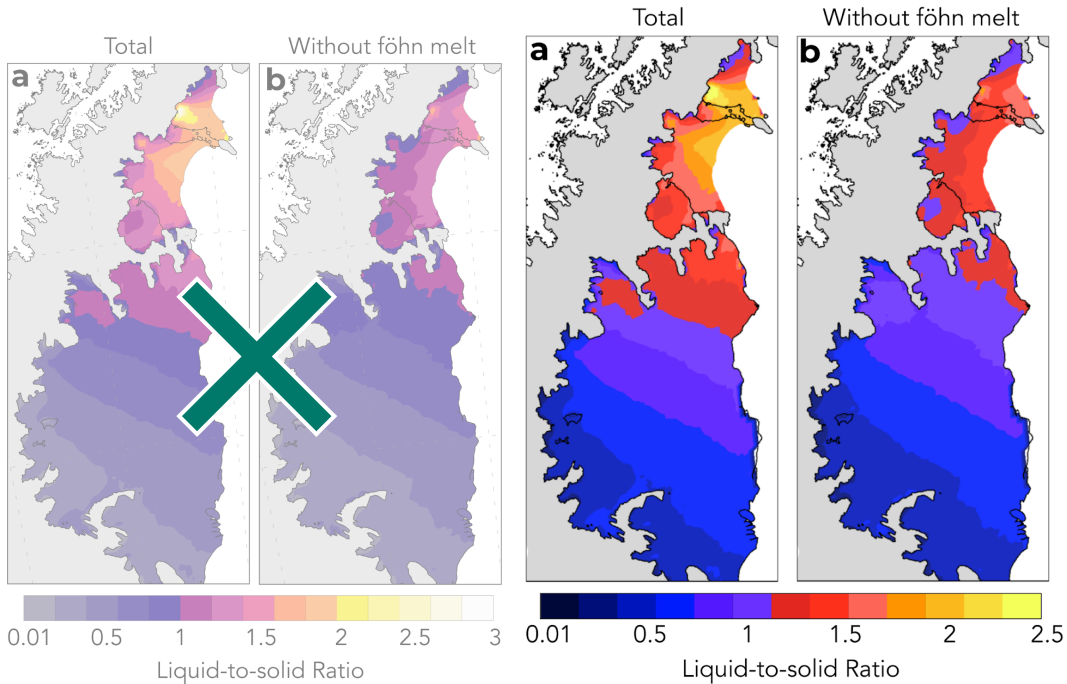


301

302 **Figure 56.** Box and whisker plots intercompare ice shelves with RACMO2-simulations from 1980-2002. Annual surface melt production  
 303 (a) all melt, (b) non-föhn melt, (c) föhn-induced melt. (d) Mean annual air temperature, (e) air temperature without föhn winds, (f) air  
 304 temperature during föhn winds. *Note:* the LAIS estimates are hypothetical after 1995, but are still resolved in the model simulations.

305

306



307



308 **Figure 67.** RACMO2 firn liquid-to-solid ratio or mean annual liquid water divided by mean annual frozen precipitation from 1979-2002  
309 for (a) total melt and (b) all liquid water except föhn-induced melt. *Note:* the LAIS estimates are hypothetical after 1995, but are still  
310 resolved in the model simulations.

#### 311 **4 Discussion**

312 The north/south temperature gradient present on the eastern AP ice shelves contributes to the differences in the ice shelf melt  
313 regime (Figure 56). Warmer ice shelves can be more vulnerable to long-term thinning and retreat that accelerate  
314 disintegration (Scambos et al., 2003; Morris and Vaughan, 2003). However, the temperature gradient alone does not  
315 explain the substantial increase in surface melt on the LAIS and LBIS relative to more southerly ice shelves. Only with the  
316 addition of föhn-induced surface melt (Figure 56c) do the LAIS and LBIS stand out significantly from the other eastern AP  
317 ice shelves (Figure 56a,b). *Temperature gradient however, could explain why föhn wind events cause less melt on more  
318 southern ice shelves and may cause super melt events on collapsed ice shelves because temperature is already elevated on  
319 more northern ice shelves prior to the effect föhn has on temperature.* With that in mind, we have examined liquid water  
320 processes on the spatio-temporal scales pertinent to AP ice shelf stability. For instance, the structural flow discontinuities or  
321 suture zones, where tributary glaciers merge together to form an ice shelf, are mechanically weak points that impact stability  
322 (Sandhager et al., 2005; Glasser and Scambos (2008); Glasser et al., 2009). These suture zones are further weakened through  
323 lateral shear depending on the difference in tributary glacier flow. All ice shelves in the region are composed of numerous  
324 outflow glaciers sutured together, and while some studies suggest this is a major contributor to ice shelf instability, only two  
325 of the ice shelves have collapsed (Borstad et al., 2016; Glasser and Scambos, 2008). Further research suggests that marine  
326 accretion of ice on the bottom of the ice shelves, specifically LCIS, may stabilise these suture zones, which may be why  
327 SCAR inlet has remained intact despite major rift formation (McGrath et al., 2014; Borstad et al., 2016).

328 The timing of surface melt and melt enhanced by föhn winds within the melt season may also provide insight into  
329 the fate of LAIS and LBIS, including why neither ice shelf collapsed in the anomalously strong 1992/93 melt season (Figure  
330 3d). Pore space within the upper snow and firn layers buffers surface melt before lakes begin to form (Polashenski et al.,  
331 2017). Late season melt is more likely to form surface melt lakes because meltwater from the preceding fall, winter, and  
332 spring has partially or completely filled available pore space. On both the LAIS and LBIS, 92% of surface melt during the  
333 1992/93 melt season occurred before January 9th when there was more pore space to buffer the anomalous surface melt than  
334 at the onsets of their collapses in late January 1995 and early February 2002, respectively (Figure 4a, c). Melt lakes were  
335 present on both ice shelves throughout the 1992/93 melt season, though melt production slowed dramatically after  
336 mid-January, 1993 (Scambos et al., 2000). The high melt rates in late November and early December 1992 on the LAIS were  
337 perhaps too early in the melt season, and after too many years of nominal melt, to form substantial melt lakes and trigger  
338 hydrofracture that season. Nevertheless, the 1992/93 melt could have preconditioned the shelf for collapse in January 1995.

339 The LBIS collapse began in February 2002 after the surface melt had returned to nominal, 1980s levels for six years. How  
340 much pore space had recovered during those six years is unknown, and an important question for future research. Satellite  
341 images of surface melt lakes indicate 11% of the ice shelf was covered in melt lakes prior to collapse (Glasser and Scambos  
342 (2008)). However, the preceding melt year (2000/2001) had low melt and high precipitation, which added additional snow  
343 and water mass to the unstable ice shelf (Leeson et al., 2017).

344 Another possible reason collapse of the LAIS and LBIS did not occur in the 92/93 melt season or other years prior  
345 to collapse was a possible misalignment of the four prerequisites for rapid collapse theorised by Massom et al., (2018). An  
346 AVHRR image of the LAIS taken on December 8, 1992, just after a series of major föhn wind events that lead to 252 mm  
347 w.e. of surface melt in the 8 days prior to the image (Figure 4a), show significant melt lakes across the LAIS, which make  
348 hydrofracture cascades possible. However, in the same image, sea ice/melange are shown to be at the calving front,  
349 protecting the front from large long period ocean waves swells that could trigger collapse. It may have been too early in the  
350 melt season to have substantial gaps in sea ice, the ocean temperature may have been too cold, ocean circulation could have  
351 helped stabilise the sea ice at the front, the föhn winds speed could have been too weak to push the ice away or may have been  
352 in the wrong direction, all of which could have not allowed a proper trigger for collapse even though substantial melt ponds  
353 were present. Even if there were years or instances that sea ice extent was low and substantial melt lakes were present, there  
354 could have been a lack of large long period ocean swells that are thought to trigger collapse.

355 Regardless of other possible contributors to ice shelf instability not considered here (e.g., basal warming melting),  
356 föhn-induced surface melt and associated melt lakes, and the off-coast wind direction likely played an important role in  
357 pushing the LAIS and LBIS past a structural tipping point. The estimated surface melt lake depth caused by the 9-day föhn  
358 melt event on the LAIS surpassed the critical melt lake depth of stability identified by model studies modelled and  
359 satellite-derived lake depths before the collapse of the LBIS (Banwell et al., 2013; Banwell et al., 2014). The LAIS was  
360 likely the same thickness (200m) or thinner at the time of collapse so the estimate of critical surface lake depth for the LBIS  
361 that is applied to the LAIS may reflect an upper limit of melt lake depth of stability for the LAIS. Melt lake depth is likely  
362 underestimated because our estimation only accounts for melt during the 9-day melt event. Melt before this time period  
363 already exceeded an average melt year by 23% (118 mm w.e.) so melt lakes probably already existed.

## 364 5 Conclusions

365 The converging lines of evidence in these results show that observed and inferred föhn-driven melt is present in sufficient  
366 amounts, and at the right locations and times, to cause extensive surface melt lakes, while the off-coast föhn wind direction  
367 pushed sea ice away from the calving front. The fact that the LAIS and LBIS collapsed catastrophically within weeks and  
368 not through long-term thinning and retreat like other ice shelves (Prince Gustav, Wordie) suggests sudden disintegration is

369 anomalous and requires forcings to match vulnerabilities (Scambos et al., 2003). We conclude that föhn winds and the  
370 associated surface melt played a significant role in the collapses of the LAIS and LBIS, while extant eastern AP ice shelves  
371 are not likely to collapse from föhn-induced melt and hydrofracture in today's current climate. We have come to these  
372 conclusions with the following forms of evidence:

373

- 374 • First, both the LAIS and LBIS are impacted by powerful melt-inducing föhn jets that affect a large spatial portion of  
375 each ice shelf and reach the ice shelf terminus. Surface melt and melt lakes near the ice shelf terminus can lead to  
376 calving front collapse and structural instability for the remaining portion of the ice shelves (Depoorter et al., 2013;  
377 Pollard et al., 2015). ~~Extant SCAR inlet and the LCIS ice shelves~~ are either not directly affected by a föhn jet, are  
378 too vast to have any significant effect near the terminus, or are too far south to experience major melt events.
- 379 • Second, strong föhn winds were present prior to and during collapse for the LAIS and LBIS. A series of three föhn  
380 events on the LAIS lasted nine days total and produced over 25% of the total annual melt for the 1994/95 melt  
381 season, while föhn was present prior to and during the collapse of the LBIS which enhanced surface melt rates.  
382 Enhanced melt, filled new and existing melt lakes above the ~~critical (1-meter) melt lake depth of stability observed~~  
383 ~~on the LBIS (1m) and modelled lake depth (5m) that could trigger large-scale hydrofracture cascades~~. The föhn  
384 winds on both ice shelves actively pushed/melted sea ice away from the calving front allowing ~~large~~ long period  
385 ocean swells to trigger large-scale hydrofracture cascades ~~on the LBIS and possibly LAIS~~, exacerbated by  
386 extensive surface melt ~~and that~~ originated from the ice shelf terminus.
- 387 • Third, in the absence of föhn wind-induced melt, the surface liquid budgets of collapsed and intact ice shelves are  
388 climatically similar, which points to föhn winds as a driver of increased surface melt and extensive melt lakes on  
389 collapsed ice shelves. The additional föhn induced-melt on the LAIS and LBIS compared to intact ice shelves  
390 helped precondition the LAIS and LBIS to produce extensive melt lakes by long-term firn densification.

391

392 This research clarifies the roles of föhn-induced melt for collapsed and extant ice shelves ~~on the eastern AP~~. Future  
393 analyses of these ice shelf collapse events using advanced firn density models coupled with ice-ocean-atmospheric coupled  
394 simulations may be useful to better understand the role of surface melt in ice shelf instability. Further, the AP föhn wind  
395 regime has remained stable over the past half-century (Laffin et al., 2021) which points to enhanced surface temperatures  
396 and increased liquid phase precipitation as more important contributors to the future surface liquid budget on remaining ice  
397 shelves and is an important area of future research (Bozkurt et al., 2020; Bozkurt et al., 2021). However, changes in climate  
398 drivers such as the Southern Annular Mode (SAM), which influences the north-south movement of the westerlies in the  
399 region, may alter the temperature and föhn occurrence that will likely enhance surface melt in locations farther south, and  
400 therefore make more southern ice shelves more vulnerable (Abram et al., 2014; Zheng et al., 2013; Lim et al., 2016; ).

401 Nevertheless, this research highlights a new understanding behind ~~surface föhn~~ melt mechanisms for ice shelf collapse and  
402 suggests that ~~extant ice shelves~~ SCAR inlet and the LCIS ~~in the region~~ may remain stable so long as surface liquid water  
403 from melt and precipitation remains within historical bounds.

404

405

406 *Author contributions.* M.K.L and C.S.Z designed the study. M.V.W. and S.M. curated the model simulation output and  
407 surface observations. M.K.L performed statistical data analysis. M.K.L. wrote the article with valuable input from all  
408 authors.

409

410 *Competing interests.* The authors declare no conflict of interest.

411

412 *Acknowledgments.* MKL was supported by the National Science Foundation (NRT-1633631) and NASA AIST  
413 (80NSSC17K0540). CSZ gratefully acknowledges support from the DOE BER ESM and SciDAC programs  
414 (DE-SC0019278, LLNL-B639667, LANL-520117). JMVW acknowledges support by PROTECT and was partly funded by  
415 the NWO (Netherlands Organisation for Scientific Research) VENI grant VI.Veni.192.083. We thank Dr. Helmut Rott for  
416 generously providing detailed in-person observations of the LAIS months before collapse. We also thank the Institute for  
417 Marine and Atmospheric research Utrecht (IMAU) for providing RACMO2 output. RACMO2 model data are available by  
418 request at <https://www.projects.science.uu.nl/iceclimate/models/antarctica.php>, however, a subset (2001-2018) of the data are  
419 hosted online at <https://zenodo.org/record/3677642#.X-pXAFNKjUI>.

## 420 **References**

- 421 Abram, N. J., Mulvaney, R., Vimeux, F., Phipps, S. J., Turner, J. and England, M. H.: Evolution of the Southern Annular  
422 Mode during the past millennium, *Nat. Clim. Chang.*, 4(7), 564–569, doi:10.1038/nclimate2235, 2014.
- 423 Adusumilli, S., Fricker, H. A., Siegfried, M. R., Padman, L., Paolo, F. S. and Ligtenberg, S. R. M.: Variable Basal Melt Rates  
424 of Antarctic Peninsula Ice Shelves, 1994–2016, *Geophys. Res. Lett.*, 45(9), 4086–4095, doi:10.1002/2017GL076652,  
425 2018.
- 426 Alley, K. E., Scambos, T. A., Miller, J. Z., Long, D. G. and MacFerrin, M.: Quantifying vulnerability of Antarctic ice shelves  
427 to hydrofracture using microwave scattering properties, *Remote Sens. Environ.*, 210, 297–306,  
428 doi:10.1016/j.rse.2018.03.025, 2018.
- 429 Banwell, A. F., MacAyeal, D. R. and Sergienko, O. V.: Breakup of the Larsen B Ice Shelf triggered by chain reaction  
430 drainage of supraglacial lakes, *Geophys. Res. Lett.*, 40(22), 5872–5876, doi:10.1002/2013GL057694, 2013.

431 Banwell, A. F., Caballero, M., Arnold, N. S., Glasser, N. F., Cathles, L. Mac and MacAyeal, D. R.: Supraglacial lakes on the  
432 Larsen B ice shelf, Antarctica, and at Paakitsoq, West Greenland: A comparative study, *Ann. Glaciol.*, 55(66), 1–8,  
433 doi:10.3189/2014AoG66A049, 2014.

~~434 Banwell, A. F., MacAyeal, D. R. and Sergienko, O. V.: Breakup of the Larsen B Ice Shelf triggered by chain reaction  
435 drainage of supraglacial lakes, *Geophys. Res. Lett.*, 40(22), 5872–5876, doi:10.1002/2013GL057694, 2013.~~

436 Banwell, A. F., Willis, I. C., MacDonald, G. J., Goodsell, B., Mayer, D. P., Powell, A. and MacAyeal, D. R.: Calving and  
437 rifting on the McMurdo Ice Shelf, Antarctica, *Ann. Glaciol.*, 58(75), 78–87, doi:10.1017/aog.2017.12, 2017.

438 Banwell, A. F., Willis, I. C., Macdonald, G. J., Goodsell, B. and MacAyeal, D. R.: Direct measurements of ice-shelf flexure  
439 caused by surface meltwater ponding and drainage, *Nat. Commun.*, 10(1), doi:10.1038/s41467-019-08522-5, 2019.

~~440 Banwell, A. F., Willis, I. C., MacDonald, G. J., Goodsell, B., Mayer, D. P., Powell, A. and MacAyeal, D. R.: Calving and  
441 rifting on the McMurdo Ice Shelf, Antarctica, *Ann. Glaciol.*, 58(75), 78–87, doi:10.1017/aog.2017.12, 2017.~~

442 Bell, R. E., Banwell, A. F., Trusel, L. D. and Kingslake, J.: Antarctic surface hydrology and impacts on ice-sheet mass  
443 balance, *Nat. Clim. Chang.*, 8(12), 1044–1052, doi:10.1038/s41558-018-0326-3, 2018.

444 Bevan, S. L., Luckman, A., Hubbard, B., Kulesa, B., Ashmore, D., Kuipers Munneke, P., O’Leary, M., Booth, A., Sevestre,  
445 H. and McGrath, D.: Centuries of intense surface melt on Larsen C Ice Shelf, *Cryosphere*, doi:10.5194/tc-11-2743-2017,  
446 2017.

447 Borstad, C., Khazendar, A., Scheuchl, B., Morlighem, M., Larour, E. and Rignot, E.: A constitutive framework for predicting  
448 weakening and reduced buttressing of ice shelves based on observations of the progressive deterioration of the remnant  
449 Larsen B Ice Shelf, *Geophys. Res. Lett.*, 43(5), 2027–2035, doi:10.1002/2015GL067365, 2016.

450 Bozkurt, D., Rondanelli, R., Marín, J. C. and Garreaud, R.: Foehn Event Triggered by an Atmospheric River Underlies  
451 Record-Setting Temperature Along Continental Antarctica, *J. Geophys. Res. Atmos.*, doi:10.1002/2017JD027796, 2018.

452 Bozkurt, D., Bromwich, D. H., Carrasco, J., Hines, K. M., Maureira, J. C. and Rondanelli, R.: Recent Near-surface  
453 Temperature Trends in the Antarctic Peninsula from Observed, Reanalysis and Regional Climate Model Data, *Adv.  
454 Atmos. Sci.*, 37(5), 477–493, doi:10.1007/s00376-020-9183-x, 2020.

455 Bozkurt, D., Bromwich, D. H., Carrasco, J. and Rondanelli, R.: Temperature and precipitation projections for the Antarctic  
456 Peninsula over the next two decades: contrasting global and regional climate model simulations, *Clim. Dyn.*,  
457 doi:10.1007/s00382-021-05667-2, 2021.

458 Braun, M. and Humbert, A.: Recent retreat of wilkins ice shelf reveals new insights in ice shelf breakup mechanisms, *IEEE  
459 Geosci. Remote Sens. Lett.*, 6(2), 263–267, doi:10.1109/LGRS.2008.2011925, 2009.

460 Bromwich, D. H. and Kurtz, D. D.: Katabatic wind forcing of the Terra Nova Bay polynya., *J. Geophys. Res.*, 89(C3),  
461 3561–3572, doi:10.1029/JC089iC03p03561, 1984.

462 Burton, J. C., Cathles, L. Mac and Wilder, W. G.: The role of cooperative iceberg capsize in ice-shelf disintegration, *Ann.*  
463 *Glaciol.*, 54(63), 84–90, doi:10.3189/2013AoG63A436, 2013.

464 Cape, M. R., Vernet, M., Skvarca, P., Marinsek, S., Scambos, T. and Domack, E.: Foehn winds link climate-driven warming  
465 to ice shelf evolution in Antarctica, *J. Geophys. Res.*, doi:10.1002/2015JD023465, 2015.

466 Carrasco, J. F., Bozkurt, D. and Cordero, R. R.: A review of the observed air temperature in the Antarctic Peninsula. Did the  
467 warming trend come back after the early 21st hiatus?, *Polar Sci.*, 28, doi:10.1016/j.polar.2021.100653, 2021.

468 Cook, A. J. and Vaughan, D. G.: Ice shelf changes on the Antarctic Peninsula Overview of areal changes of the ice shelves  
469 on the Antarctic Peninsula over the past 50 years Ice shelf changes on the Antarctic Peninsula, *TCD*, 3, 579–630  
470 [online] Available from: [www.the-cryosphere-discuss.net/3/579/2009/](http://www.the-cryosphere-discuss.net/3/579/2009/), 2009.

471 Datta, R. T., Tedesco, M., Fettweis, X., Agosta, C., Lhermitte, S., Lenaerts, J. T. M. and Wever, N.: The Effect of  
472 Foehn Induced Surface Melt on Firn Evolution Over the Northeast Antarctic Peninsula, *Geophys. Res. Lett.*,  
473 2018GL080845, doi:10.1029/2018GL080845, 2019.

474 Depoorter, M. A., Bamber, J. L., Griggs, J. A., Lenaerts, J. T. M., Ligtenberg, S. R. M., Van Den Broeke, M. R. and Moholdt,  
475 G.: Calving fluxes and basal melt rates of Antarctic ice shelves, *Nature*, 502(7469), 89–92, doi:10.1038/nature12567,  
476 2013.

477 Doake, C. S. M., Corr, H. F. J., Rott, H., Skvarca, P. and Young, N. W.: Breakup and conditions for stability of the northern  
478 Larsen Ice Shelf, *Antarctica, Nature*, 391, 778–780, 1988.

479 Elvidge, A. D., Kuipers Munneke, P., King, J. C., Renfrew, I. A. and Gilbert, E.: Atmospheric Drivers of Melt on Larsen C  
480 Ice Shelf: Surface Energy Budget Regimes and the Impact of Foehn, *J. Geophys. Res. Atmos.*, 125(17),  
481 doi:10.1029/2020JD032463, 2020.

482 Elvidge, A. D., Renfrew, I. A., King, J. C., Orr, A., Lachlan-Cope, T. A., Weeks, M. and Gray, S. L.: Foehn jets over the  
483 Larsen C Ice Shelf, *Antarctica, Q. J. R. Meteorol. Soc.*, 141(688), 698–713, doi:10.1002/qj.2382, 2015.

484 Glasser, N. F. and Scambos, T. A.: A structural glaciological analysis of the 2002 Larsen B ice-shelf collapse, *J. Glaciol.*,  
485 54(184), 3–16, doi:10.3189/002214308784409017, 2008.

486 Glasser, N. F., Kulesa, B., Luckman, A., Jansen, D., King, E. C., Sammonds, P. R., Scambos, T. A. and Jezek, K. C.:  
487 Surface structure and stability of the Larsen C ice shelf, *Antarctic Peninsula.*, 2009.

488 Grosvenor, D. P., King, J. C., Choularton, T. W. and Lachlan-Cope, T.: Downslope föhn winds over the antarctic peninsula  
489 and their effect on the larsen ice shelves, *Atmos. Chem. Phys.*, 14(18), 9481–9509, doi:10.5194/acp-14-9481-2014,  
490 2014.

491 Gudmundsson, G. H.: Ice-shelf buttressing and the stability of marine ice sheets, *Cryosphere*, 7(2), 647–655,  
492 doi:10.5194/tc-7-647-2013, 2013. Holland, P. R., Corr, H. F. J., Pritchard, H. D., Vaughan, D. G., Arthern, R. J., Jenkins,  
493 A. and Tedesco, M.: The air content of Larsen Ice Shelf, *Geophys. Res. Lett.*, doi:10.1029/2011GL047245, 2011.

494 Hubbard, B., Luckman, A., Ashmore, D. W., Bevan, S., Kulesa, B., Kuipers Munneke, P., Philippe, M., Jansen, D., Booth,  
495 A., Sevestre, H., Tison, J. L., O'Leary, M. and Rutt, I.: Massive subsurface ice formed by refreezing of ice-shelf melt  
496 ponds, *Nat. Commun.*, 7, doi:10.1038/ncomms11897, 2016.

497 King, J. C., Gadian, A., Kirchgaessner, A., Kuipers Munneke, P., Lachlan-Cope, T. A., Orr, A., Reijmer, C., van den Broeke,  
498 M. R., van Wessem, J. M. and Weeks, M.: Validation of the summertime surface energy budget of Larsen C Ice Shelf  
499 (Antarctica) as represented in three high-resolution atmospheric models, *J. Geophys. Res.*, 120(4), 1335–1347,  
500 doi:10.1002/2014JD022604, 2015.

501 King, J. C., Kirchgaessner, A., Bevan, S., Elvidge, A. D., Kuipers Munneke, P., Luckman, A., Orr, A., Renfrew, I. A. and van  
502 den Broeke, M. R.: The Impact of Föhn Winds on Surface Energy Balance During the 2010–2011 Melt Season Over  
503 Larsen C Ice Shelf, Antarctica, *J. Geophys. Res. Atmos.*, doi:10.1002/2017JD026809, 2017.

504 Kirchgaessner, A., King, J. C. and Anderson, P. S.: The Impact of Föhn Conditions Across the Antarctic Peninsula on Local  
505 Meteorology Based on AWS Measurements, *J. Geophys. Res. Atmos.*, 126(4), doi:10.1029/2020JD033748, 2021.

506 Kuipers Munneke, P., Luckman, A. J., Bevan, S. L., Smeets, C. J. P. P., Gilbert, E., van den Broeke, M. R., Wang, W.,  
507 Zender, C., Hubbard, B., Ashmore, D., Orr, A., King, J. C. and Kulesa, B.: Intense Winter Surface Melt on an Antarctic  
508 Ice Shelf, *Geophys. Res. Lett.*, doi:10.1029/2018GL077899, 2018.

509 Kuipers Munneke, P., Van Den Broeke, M. R., King, J. C., Gray, T. and Reijmer, C. H.: Near-surface climate and surface  
510 energy budget of Larsen C ice shelf, Antarctic Peninsula, *Cryosphere*, 6(2), 353–363, doi:10.5194/tc-6-353-2012, 2012.

511 Laffin, M. K., Zender, C. S., Singh, S., Van Wessem, J. M., Smeets, C. J. P. P. and Reijmer, C. H.: Climatology and Evolution  
512 of the Antarctic Peninsula Föhn Wind-Induced Melt Regime From 1979–2018, *J. Geophys. Res. Atmos.*, 126(4),  
513 doi:10.1029/2020JD033682, 2021.

514 Larour, E., Rignot, E., Poinelli, M. and Scheuchl, B.: Physical processes controlling the rifting of Larsen C Ice Shelf,  
515 Antarctica, prior to the calving of iceberg A68, *Proc. Natl. Acad. Sci. U. S. A.*, 118(40), doi:10.1073/pnas.2105080118,  
516 2021.

517 Leeson, A. A., Forster, E., Rice, A., Gourmelen, N. and van Wessem, J. M.: Evolution of Supraglacial Lakes on the Larsen B  
518 Ice Shelf in the Decades Before it Collapsed, *Geophys. Res. Lett.*, 47(4), doi:10.1029/2019GL085591, 2020.

519 Leeson, A. A., Van Wessem, J. M., Ligtenberg, S. R. M., Shepherd, A., Van Den Broeke, M. R., Killick, R., Skvarca, P.,  
520 Marinsek, S. and Colwell, S.: Regional climate of the Larsen B embayment 1980-2014, *J. Glaciol.*, 63(240), 683–690,  
521 doi:10.1017/jog.2017.39, 2017.

522 Lenaerts, J. T. M., Lhermitte, S., Drews, R., Ligtenberg, S. R. M., Berger, S., Helm, V., Smeets, C. J. P. P., Broeke, M. R. V.  
523 Den, Van De Berg, W. J., Van Meijgaard, E., Eijkelboom, M., Eisen, O. and Pattyn, F.: Meltwater produced by  
524 wind-albedo interaction stored in an East Antarctic ice shelf, *Nat. Clim. Chang.*, doi:10.1038/nclimate3180, 2017.

525 Lhermitte, S., Sun, S., Shuman, C., Wouters, B., Pattyn, F., Wuite, J., Berthier, E. and Nagler, T.: Damage accelerates ice  
526 shelf instability and mass loss in Amundsen Sea Embayment, *Sci. Libr. Ser.*, 117,  
527 doi:10.1073/pnas.1912890117/-/DCSupplemental.y, 2020.

528 Lim, E. P., Hendon, H. H., Arblaster, J. M., Delage, F., Nguyen, H., Min, S. K. and Wheeler, M. C.: The impact of the  
529 Southern Annular Mode on future changes in Southern Hemisphere rainfall, *Geophys. Res. Lett.*, 43(13), 7160–7167,  
530 doi:10.1002/2016GL069453, 2016.

531 Luckman, A., Elvidge, A., Jansen, D., Kulesa, B., Kuipers Munneke, P., King, J. and Barrand, N. E.: Surface melt and  
532 ponding on Larsen C Ice Shelf and the impact of föhn winds, *Antarct. Sci.*, doi:10.1017/S0954102014000339, 2014.

533 Massom, R. A., Scambos, T. A., Bennetts, L. G., Reid, P., Squire, V. A. and Stammerjohn, S. E.: Antarctic ice shelf  
534 disintegration triggered by sea ice loss and ocean swell, *Nature*, 558(7710), 383–389, doi:10.1038/s41586-018-0212-1,  
535 2018.

536 McGrath, D., Steffen, K., Holland, P. R., Scambos, T., Rajaram, H., Abdalati, W. and Rignot, E.: The structure and effect of  
537 suture zones in the Larsen C Ice Shelf, *Antarctica, J. Geophys. Res. Earth Surf.*, 119(3), 588–602,  
538 doi:10.1002/2013JF002935, 2014.

539 Morris, E. M. and Vaughan, D. G.: Spatial and Temporal Variation of Surface Temperature on the Antarctic Peninsula and  
540 the Limit of Viability of Ice Shelves, *Antarct. Res. Ser.*, 79, 61–68, doi:10.1029/079ARS05, 2003.

541 Mulvaney, R., Abram, N. J., Hindmarsh, R. C. A., Arrowsmith, C., Fleet, L., Triest, J., Sime, L. C., Alemany, O. and Foord,  
542 S.: Recent Antarctic Peninsula warming relative to Holocene climate and ice-shelf history, *Nature*, 489(7414), 141–144,  
543 doi:10.1038/nature11391, 2012.

544 Munneke, P. K., Ligtenberg, S. R. M., Van Den Broeke, M. R. and Vaughan, D. G.: Firm air depletion as a precursor of  
545 Antarctic ice-shelf collapse, *J. Glaciol.*, 60(220), 205–214, doi:10.3189/2014JoG13J183, 2014.

546 Polashenski, C., Golden, K. M., Perovich, D. K., Skillingstad, E., Arnsten, A., Stwertka, C. and Wright, N.: Percolation  
547 blockage: A process that enables melt pond formation on first year Arctic sea ice, *J. Geophys. Res. Ocean.*, 122(1),  
548 413–440, doi:10.1002/2016JC011994, 2017.

549 Pollard, D., DeConto, R. M. and Alley, R. B.: Potential Antarctic Ice Sheet retreat driven by hydrofracturing and ice cliff  
550 failure, *Earth Planet. Sci. Lett.*, 412, 112–121, doi:10.1016/j.epsl.2014.12.035, 2015.

551 Pritchard, H. D., Ligtenberg, S. R. M., Fricker, H. A., Vaughan, D. G., Van Den Broeke, M. R. and Padman, L.: Antarctic  
552 ice-sheet loss driven by basal melting of ice shelves, *Nature*, 484(7395), 502–505, doi:10.1038/nature10968, 2012.

553 Qiao, G., Li, Y., Guo, S. and Ye, W.: Evolving instability of the scar inlet ice shelf based on sequential landsat images  
554 spanning 2005-2018, *Remote Sens.*, 12(1), doi:10.3390/RS12010036, 2020.

555 Rack, W. and Rott, H.: Pattern of retreat and disintegration of the Larsen B ice shelf, *Antarctic Peninsula, Ann. Glaciol.*, 39,  
556 505–510 [online] Available from: <https://www.cambridge.org/core>, 2004.



557 Rignot, E., Jacobs, S., Mouginot, B. and Scheuchl, B.: Ice-Shelf Melting Around Antarctica, *Science* (80-. ), 341(6143),  
558 263–266, doi:10.1126/science.1237966, 2013.Rignot, E., Casassa, G., Gogineni, P., Krabill, W., Rivera, A. and Thomas,  
559 R.: Accelerated ice discharge from the Antarctic Peninsula following the collapse of Larsen B ice shelf, *Geophys. Res.*  
560 *Lett.*, 31(18), doi:10.1029/2004GL020697, 2004.

561 Robel, A. A. and Banwell, A. F.: A Speed Limit on Ice Shelf Collapse Through Hydrofracture, *Geophys. Res. Lett.*, 46(21),  
562 12092–12100, doi:10.1029/2019GL084397, 2019.Rott, H., Rack, W., Nagler, T. and Skvarca, P.: Climatically induced  
563 retreat and collapse of norther Larsen Ice Shelf, Antarctic Peninsula, *Ann. Glaciol.*, 27, 86–92,  
564 doi:10.3189/s0260305500017262, 1998.

565 Sandhäger, H., Rack, W. and Jansen, D.: Model investigations of Larsen B Ice Shelf dynamics prior to the breakup. [online]  
566 Available from: <http://www.uib.no/People/ngfls/frisp/Rep16/sandhageretal.pdf>, 2005.

567 Scambos, T. A., Bohlander, J. A., Shuman, C. A. and Skvarca, P.: Glacier acceleration and thinning after ice shelf collapse in  
568 the Larsen B embayment, Antarctica, *Geophys. Res. Lett.*, 31(18), doi:10.1029/2004GL020670, 2004.

569 Scambos, T. A., Hulbe, C., Fahnestock, M. and Bohlander, J.: The link between climate warming and break-up of ice shelves  
570 in the Antarctic Peninsula, *J. Glaciol.*, 46(154), 516–530, doi:10.3189/172756500781833043, 2000.

571 Scambos, T., Hulbe, C. and Fahnestock, M.: Climate-Induced Ice Shelf Disintegration in the Antarctic Peninsula, pp. 79–92.,  
572 2003.

573 Schodlok, M. P., Menemenlis, D. and Rignot, E. J.: Ice shelf basal melt rates around Antarctica from simulations and  
574 observations, *J. Geophys. Res. Ocean.*, 121(2), 1085–1109, doi:10.1002/2015JC011117, 2016.

575 Trusel, L. D., Frey, K. E., Das, S. B., Karnauskas, K. B., Kuipers Munneke, P., Van Meijgaard, E. and Van Den Broeke, M.  
576 R.: Divergent trajectories of Antarctic surface melt under two twenty-first-century climate scenarios, *Nat. Geosci.*,  
577 8(12), 927–932, doi:10.1038/ngeo2563, 2015.

578 Trusel, L. D., Frey, K. E., Das, S. B., Munneke, P. K. and Van Den Broeke, M. R.: Satellite-based estimates of Antarctic  
579 surface meltwater fluxes, *Geophys. Res. Lett.*, 40(23), 6148–6153, doi:10.1002/2013GL058138, 2013.

580 Turton, J. V., Kirchgassner, A., Ross, A. N. and King, J. C.: Does high-resolution ~~modelling~~ modeling improve the spatial  
581 analysis of föhn flow over the Larsen C Ice Shelf?, *Weather*, 72(7), doi:10.1002/wea.3028, 2017.

582 Turton, J. V., Kirchgassner, A., Ross, A. N. and King, J. C.: The spatial distribution and temporal variability of föhn winds  
583 over the Larsen C ice shelf, Antarctica, *Q. J. R. Meteorol. Soc.*, doi:10.1002/qj.3284, 2018.

584 van den Broeke, M.: Strong surface melting preceded collapse of Antarctic Peninsula ice shelf, *Geophys. Res. Lett.*, 32(12),  
585 1–4, doi:10.1029/2005GL023247, 2005.

586 Vaughan, D. G., Marshall, G. J., Connolley, W. M., Parkinson, C., Mulvaney, R., Hodgson, D. A., King, J. C., Pudsey, C. J.  
587 and Turner, J.: Recent rapid regional climate warming on the Antarctic Peninsula, *Clim. Change*, 60(3), 243–274,  
588 doi:10.1023/A:1026021217991, 2003.

- 589 Wang, W., Zender, C. S., van As, D., Fausto, R. S. and Laffin, M. K.: Greenland Surface Melt Dominated by Solar and  
590 Sensible Heating, *Geophys. Res. Lett.*, 48(7), doi:10.1029/2020GL090653, 2021.
- 591 Wang, X., Zhang, Z., Wang, X., Vihma, T., Zhou, M., Yu, L., Uotila, P. and Sein, D. V.: Impacts of strong wind events on sea  
592 ice and water mass properties in Antarctic coastal polynyas, *Clim. Dyn.*, 57(11–12), 3505–3528,  
593 doi:10.1007/s00382-021-05878-7, 2021.
- 594 Wiesenekker, J. M., Munneke, P. K., van den Broeke, M. R. and Paul Smeets, C. J. P.: A multidecadal analysis of Föhn  
595 winds over Larsen C ice shelf from a combination of observations and modeling, *Atmosphere (Basel)*, 9(5),  
596 doi:10.3390/atmos9050172, 2018.
- 597 Zheng, F., Li, J., Clark, R. T. and Nnamchi, H. C.: Simulation and projection of the Southern Hemisphere annular mode in  
598 CMIP5 models, *J. Clim.*, 26(24), 9860–9879, doi:10.1175/JCLI-D-13-00204.1, 2013.